## Accelerated Publications

# Stability for Function Trade-Offs in the Enolase Superfamily "Catalytic Module"[†,‡]

Ray A. Nagatani,[§,||] Ana Gonzalez,[⊥] Brian K. Shoichet,[||,@] Linda S. Brinen,[||,#] and Patricia C. Babbitt*,[§,||,@]

*Departments of Biopharmaceutical Science, Pharmaceutical Chemistry, and Cellular and Molecular Pharmacology and Institute for Quantitative Biomedical Research, University of California, San Francisco, 1700 4th Street, Byers Hall, Box 2550, Room 508E, San Francisco, California 94158, and Stanford Synchrotron Radiation Laboratory, Stanford Linear Accelerator Center, 2575 Sand Hill Road, MS99, Menlo Park, California 94025*

ABSTRACT: Enzyme catalysis reflects a dynamic interplay between charged and polar active site residues that facilitate function, stabilize transition states, and maintain overall protein stability. Previous studies show that substituting neutral for charged residues in the active site often significantly stabilizes a protein, suggesting a stability trade-off for functionality. In the enolase superfamily, a set of conserved active site residues (the "catalytic module") has repeatedly been used in nature in the evolution of many different enzymes for the performance of unique overall reactions involving a chemically diverse set of substrates. This catalytic module provides a robust solution for catalysis that delivers the common underlying partial reaction that supports all of the different overall chemical reactions of the superfamily. As this module has been so broadly conserved in the evolution of new functions, we sought to investigate the extent to which it follows the stability–function trade-off. Alanine substitutions were made for individual residues, groups of residues, and the entire catalytic module of *o*-succinylbenzoate synthase (OSBS), a member of the enolase superfamily from *Escherichia coli*. Of six individual residue substitutions, four (K131A, D161A, E190A, and D213A) substantially increased protein stability (by 0.46–4.23 kcal/mol), broadly consistent with prediction of a stability–activity trade-off. The residue most conserved across the superfamily, E190, is by far the most destabilizing. When the individual substitutions were combined into groups (as they are structurally and functionally organized), nonadditive stability effects emerged, supporting previous observations that residues within the module interact as two functional groups within a larger catalytic system. Thus, whereas the multiple-mutant enzymes D161A/E190A/D213A and K131A/K133A/D161A/ E190A/D213A/K235A (termed 3KDED) are stabilized relative to the wild-type enzyme (by 1.77 and 3.68 kcal/mol, respectively), the net stabilization achieved in both cases is much weaker than what would be predicted if their stability contributions were additive. Organization of the catalytic module into systems that mitigate the expected stability cost due to the presence of highly charged active site residues may help to explain its repeated use for the evolution of many different functions.

The catalytic function of enzymes often depends upon a specific architecture of charged or polar residues in the proximity of each other. By adopting preorganized geometries that are energetically unfavorable, these residues are able to orient substrates through binding interactions, stabilize high-energy transition states, and provide the flexibility necessary for substrate and product turnover (*1, 2*). Thus, enzyme catalysis reflects a dynamic interplay between protein stability and protein function. While these high-energy conformations of active site residues often destabilize the global stability of the enzyme through electrostatic or steric repulsion, results from several investigations have shown that this interplay is an essential element of enzyme catalysis. Experiments with the enzyme lysozyme showed that substitution of charged catalytic residues with neutral nonpolar residues increases stability, though catalytic function is lost (*3*). Antibiotic resistant mutants of β-lactamase that have evolved in nature are destabilized relative to the wild-type enzyme, yet have a selective advantage because of their increased activity on cephalosporin substrates (*4*). Substituting residues in either the positively charged active site of the enzyme barnase or the negatively charged binding site of its inhibitor barstar has been shown to improve stability
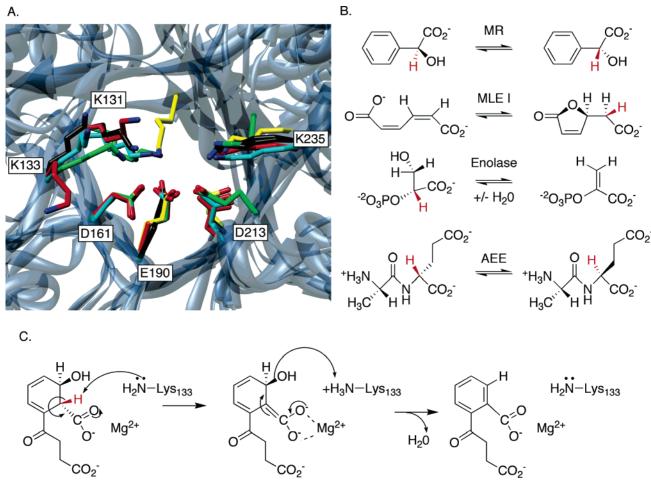
FIGURE 1: (A) Superposition of several members of the enolase superfamily members. The active site residues of each protein are color-coded as follows: black for *o*-succinylbenzoate synthase (PDB entry 1fhv), green for mandelate racemase (PDB entry 2mnr), cyan for muconate lactonizing enzyme (PDB entry 1muc), gold for enolase (PDB entry 1ebh), and red for L-Ala-D/L-Glu epimerase (PDB entry 1jpm). Active site residues are labeled using numbering from OSBS. (B) Reactions performed by MR, MLE, enolase, and AEE. (C) Reaction performed by OSBS. Molecular graphics images were produced using the UCSF Chimera package from the Resource for Biocomputing, Visualization, and Informatics at the University of California, San Francisco (supported by NIH Grant P41 RR-01081) (*47*).

at the expense of reduced activity, partly due to reducing electrostatic repulsion between catalytic residues (*5, 6*).

The stability−activity trade-off has consequences in the molecular evolution of enzyme structures (*7−9*). In part to compensate for destabilization incurred from charged catalytic residues or local structural variations between divergent enzymes, systems of catalytic residues that can mitigate the stability cost may be conserved in enzyme families. For example, serine proteases use a conserved catalytic triad of residues to hydrolyze peptide amide bonds (*10*). The geometry of this catalytic system is conserved even across different protein folds and is the foundation for the catalytic mechanism, with specificity for individual substrates conferred by unique binding elements that distinguish each enzyme. Similarly, enzymes within mechanistically diverse enzyme superfamilies (*11*) use highly conserved active site architectures (or "catalytic modules") that have retained the ability to catalyze a fundamental partial reaction (or other chemical capability) that leads to the stabilization of a common type of intermediate in all of the divergent enzymes in the superfamily.

Residues within such catalytic modules generally maintain a conserved geometry in many different structural contexts (i.e., divergent enzymes in a family, different enzyme folds) despite the significant predicted destabilization caused by

their inclusion (*12−14*). Does the catalytic module design offer a robust solution for preorganizing charged resides in a conformation that mitigates the stability cost for providing function? To answer this question, we have investigated the stability−function trade-off within the context of catalytic module residues that are conserved across all members of the mechanistically diverse enolase superfamily.

The enolase superfamily is a well-characterized superfamily of hundreds of enzymes that catalyze a chemically diverse range of different overall reactions (*15*). To date, 14 reactions performed by superfamily members have been characterized, and many more candidates have been identified that are likely to perform additional functions. Although these overall reactions range from dehydration to cycloisomerization, all members use a catalytic module of oppositely charged residues to abstract a proton from a common substrate substructure and stabilize the resulting endiolate high-energy intermediate (*16*) (Figure 1B). In the catalytic module, the conserved residues can be viewed as forming two systems that facilitate catalytic function. One system is involved in substrate orientation and transition state stabilization. The other system abstracts the substrate proton to form the transition state. The first system is comprised of three acidic residues that coordinate a divalent metal ion that plays a role in orienting the carboxylic acid substructure common

to all superfamily ligands. These residues and the metal ion are present in all members of the superfamily and exhibit few substitutions across the divergent set. The negatively charged residues of this system are sandwiched between two sets of weakly basic residues that comprise the second system (Figure 1A). In this system, the weakly basic residues abstract a proton α to the conserved carboxylic acid substructure, forming an endiolate high-energy intermediate that is stabilized through interaction with the metal ion of the first system. This second system exhibits more structural and chemical variation across the superfamily than the first, distinguishing at least three different subgroups within the superfamily (*17*).

Electrostatic calculations have suggested that the juxtaposition of these charged residues in the enolase superfamily catalytic module leads to significant electrostatic destabilization (*13*, *14*). On the basis of these conclusions, it is somewhat surprising that the geometry and chemical characteristics of this catalytic module have been used repeatedly by nature in the evolution of different functions, especially since several other architectures that perform similar proton abstraction chemistry have been observed in other biological systems (*18*, *19*). Indeed, even other superfamilies from different fold classes unrelated to the enolase superfamily have utilized similar catalytic architectures and strategies to perform this same fundamental partial reaction (*20*, *21*). The widespread conservation of the enolase superfamily catalytic module across the superfamily (and in other superfamilies) suggests instead that the module is a robust solution that has been commonly used in evolution to obtain catalytic functionality at an acceptable cost to destabilization.

To investigate quantitatively the structure−function trade-off for the catalytic module of the enolase superfamily, we performed alanine substitution of the component residues of *o*-succinylbenzoate synthase (OSBS)[1] from *Escherichia coli*. The OSBS from *E. coli* catalyzes the dehydration of 2-succinyl-6-hydroxy-2,4-cyclohexadiene-1-carboxylate (SHCHC) to *o*-succinylbenzoate (OSB) (Figure 1C), a reaction that is essential for anaerobic respiration (*22*). The OSBS from *E. coli* is a monomeric protein for which a wild-type structure is available (*23*). It is a useful system for addressing stability−function trade-offs in the enolase superfamily because its overall reaction mainly relies upon the proton abstraction step provided by the catalytic module to proceed to completion (Figure 1C), without the complications introduced by additional partial reactions required for the performance of the different overall reactions catalyzed by other members of the superfamily. Here, we investigate the thermostability of wild-type OSBS and of alanine-substituted mutants of the catalytic module residues, both as point mutants and as combinations that cover the entire catalytic module and the two systems of catalytic residues within the module. To gain additional insight into the structural

mechanisms of stabilization, we determined the crystal structure of the most thermostable mutant.

This is the first analysis of stability−function trade-offs applied to an entire active site system conserved across hundreds of different enzymes. The results provide information about the robustness of such systems for natural enzyme evolution and for engineering new catalysts in vitro.

## METHODS

*Site-Directed Mutagenesis.* The 0.96 kb *menC* gene from *E. coli* MG1655, cloned into a pET15b expression vector (Novagen, San Diego, CA), a generous gift from J. Gerlt, was used for all site-directed mutagenesis experiments. The QuickChange site-directed mutagenesis method (Stratagene, La Jolla, CA) was used to introduce point mutations. Each mutation was confirmed by DNA sequencing.

*Biosynthesis of SHCHC.* SHCHC was synthesized as described previously from chorismic acid (*24*), using the coupled actions of isochorismate mutase and SHCHC synthase. The compound was then purified as described previously (*25*, *26*).

*Spectrophotometric Assay.* OSBS activity was assayed at pH 8 as previously described (*25*) using 250 nM SHCHC in an assay buffer containing 50 mM Tris-HCl and 5 mM $MgCl_2$ (pH 8).

*Isolation of Wild-Type and Alanine-Mutant OSBS from E. coli. E. coli* BL21(DE3) cells were transformed with the plasmid and grown at 37 °C in LB medium for 18 h without induction. Cells were resuspended in 30 mL of binding buffer [10 mM Tris-HCl (pH 8) containing 5 mM imidazole, 0.5 M NaCl, and 5 mM $MgCl_2$] and then disrupted by sonication. Following centrifugation, the supernatant was loaded onto a HisTrap 5 mL HP column (GE Biosciences, Piscataway, NJ) that had been equilibrated with binding buffer. Following a wash step with 5 column volumes of buffer, wild-type OSBS and mutants were eluted using a linear imidazole gradient [from 0 to 1 M imidazole in 10 mM Tris-HCl (pH 8) containing 5 mM $MgCl_2$ and 0.5 M NaCl]. Fractions containing wild-type OSBS or mutant proteins were then dialyzed against 1 L of phosphate-buffered saline. The His tag was removed by incubation with 1 unit of thrombin/mg of OSBS for 72 h at 4 °C. The dialyzed protein was then loaded onto a DEAE anion exchange column (GE Biosciences) and eluted with a linear NaCl gradient [from 0 to 0.5 M NaCl in 10 mM Tris-HCl (pH 8.0) containing 5 mM $MgCl_2$]. Fractions containing homogeneous wild-type OSBS or mutants were pooled and concentrated using an Amicon 30 kDa molecular mass cutoff centrifugal filter. The purity of the samples was verified using SDS−PAGE, which showed a single band (data not shown).

*Enzyme Stability Analysis by Circular Dichroism (CD).* CD experiments were conducted using a Jasco J-715 spectropolarimeter with a Jasco PCT-348WI Peltier-effect temperature controller. Quartz cells with a path length of 1 cm (Hellma, Inc., Plainview, NY) were used for all measurements. The temperature was monitored and controlled using an in-cell thermometer and stir bar.

Thermal denaturation of wild-type OSBS and all mutant proteins was carried out in a 50 mM $KP_i$, 200 mM KCl, 20% ethylene glycol buffer (pH 8). For the experiment aimed at monitoring the tertiary structure, a buffer containing 50 mM $KP_i$, 200 mM KCl, and 45% ethylene glycol (pH 8.5)

---

[1] Abbreviations: AEE, L-Ala-D/L-Glu epimerase; CD, circular dichroism; $\Delta C_p$, change in the constant-pressure heat capacity; $\Delta\Delta G_u$, change in the free energy of unfolding; MLE, muconate lactonizing enzyme; MR, mandelate racemase; OSBS, *o*-succinylbenzoate synthase; $\Delta S_{u,WT}$, van't Hoff entropy of unfolding; SHCHC, 2-succinyl-6-hydroxy-2,4-cyclodiene-1-carboxylate; $T_M$, temperature of melting; $\Delta T_M$, difference between the mutant $T_M$ and the wild-type $T_M$.

was used. Denaturation was monitored between 293 and 343 K, with a heating rate of 2 °C/min.

All proteins were monitored for helical content by CD in the far-UV region (223 nm) at an enzyme concentration of 0.02 mg/mL. The wild-type protein was also monitored for tertiary structure by CD in the near-UV region (285 nm) at an enzyme concentration of 0.1 mg/mL.

Thermal denaturation was analyzed using EXAM (*27*) to calculate all melting temperatures ($T_M$) and van't Hoff enthalpy of unfolding ($\Delta H_{VH}$) values. Melting curve baselines were fixed on the basis of initial predictions made by EXAM. With the exception of mutants E190A and 3KDED, the experimentally derived change in heat capacity ($\Delta C_p$) for wild-type OSBS (3.2 kcal mol$^{-1}$ K$^{-1}$) was used as an input parameter for the curve fitting program in EXAM. For E190A and 3KDED, each mutant's experimentally derived $\Delta C_p$ was used as an input parameter. Each reported melting temperature is the average of at least three independent experiments.

The change in the free energy of unfolding ($\Delta\Delta G_u$) was calculated using the method of Schellman (*28*), where $\Delta\Delta G_u = \Delta T_M \Delta S_{u,WT}$. For the E190A and 3KDED mutants, the change in free energy of unfolding was also calculated using the equation $\Delta G = \Delta H_{wt} - T\Delta S_{wt} + \Delta C_p[T - T_{wt} - T \ln(T/T_{wt})]$, which takes differences in $\Delta C_p$ into account. Increases in melting temperature indicate increased stability, resulting in a positive $\Delta\Delta G_u$. The $\Delta C_p$ of the wild-type and selected OSBS mutant proteins was determined from van't Hoff plots in the presence of varying amounts of freshly prepared urea as described below.

*Calculation of $\Delta C_p$.* Wild-type OSBS and mutants that were highly stabilized (E190A and 3KDED) were reversibly denatured by temperature in a 50 mM KP$_i$, 200 mM KCl, 20% ethylene glycol buffer (pH 8) with ultrapure urea (Fluka, St. Louis, MO) added to a total concentration of up to 2 M. Samples in each buffer were then analyzed using far-UV CD. Thermal denaturation was analyzed using EXAM to calculate all melting temperatures ($T_M$) and van't Hoff enthalpy of unfolding ($\Delta H_{VH}$) values. Melting curve baselines were fixed on the basis of initial predictions made by EXAM. Because the $\Delta C_p$ was unknown prior to the experiment, an estimated $\Delta C_p$ value of 1.7 kcal mol$^{-1}$ K$^{-1}$ was used as an input parameter for the curve fitting program in EXAM. This parameter value was found to consistently provide robust curve fitting of the data across the different denaturant concentrations. The average $T_M$ of each protein was plotted against the average $\Delta H_{VH}$ at each urea concentration to generate a van't Hoff plot, where $\Delta C_p$ is represented by the slope (Figure 3). For each van't Hoff plot, every point reflects at least three melts at each urea concentration.

*Crystal Growth and Structure Determination.* Crystals of the E190A mutant were grown by vapor diffusion in sitting drops equilibrated over 0.1 M MES (pH 5.8), 75 mM sodium molybdate, and 25% (v/v) PEG 4000. The initial concentration of protein in the drop was 6 mg/mL. Crystals appeared over a few days after equilibration at 18 °C. Before data collection, crystals were immersed in a cryoprotectant solution of 20% (v/v) ethylene glycol, 0.1 M MES (pH 5.8), 75 mM sodium molybdate, and 25% (v/v) PEG 4000.

Diffraction data were collected on cryo-cooled crystals on beamline BL 9-1 at the Stanford Synchrotron Radiation
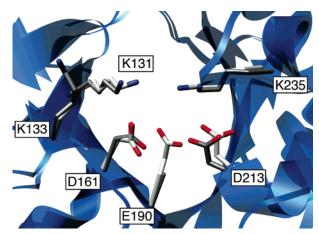


FIGURE 2: Structural superposition of the OSBS wild-type structure (light gray) and the E190A mutant structure (dark gray).
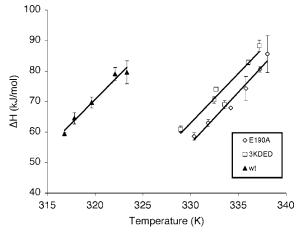


FIGURE 3: van't Hoff plots for wild-type OSBS (▲), E190A (◇), and 3KDED (□).

Laboratory. The data set was measured from a single crystal. Reflections were indexed, integrated, and scaled using MOSFLM (*29*) and SCALA (*30*). For the E190A structure, the space group was $P2_1$; the unit cell was refined to the following dimensions: $a = 69.47$ Å, $b = 77.39$ Å, $c = 110.68$ Å, and $\beta = 90.08°$. The data set statistics are summarized in Table 2.

The structure was determined by the Molecular Replacement method, using MOLREP (*30*, *31*). Four molecules were located in the asymmetric unit. Refinement of the structure was carried out with REFMAC5 (*30*, *32*). Independent rigid body refinement of each of the four molecules was followed by alternating cycles of restrained refinement and water molecular search using ARP/wARP (*33*). The model was inspected and rebuilt with COOT (*34*). TLS refinement (*35*) was carried out at the end of the refinement process.

## RESULTS

*Effects of Alanine Substitution on Activity.* All alanine-substituted OSBS mutants were assayed for the ability to catalyze the dehydration of SHCHC by monitoring the loss of substrate. None of the mutants displayed detectable activity.

*Reversible Denaturation and Two-State Behavior of Wild-Type OSBS.* OSBS wild-type enzyme was reversibly denatured by temperature and analyzed by far-UV and near-UV CD. The loss of helical content and tertiary structure was fit

Table 1: Melting Temperatures and $\Delta T_M$, $\Delta H$, and $\Delta\Delta G_u$ Values for Wild-Type OSBS and Mutants[a]

|  | melting temp (°C) | $\Delta T_M$ | $\Delta H$ (kcal/mol) | $\Delta\Delta G_u$ (kcal/mol) |
|---|---|---|---|---|
| wild type | 50.8 | 0.0 | 86.1 | 0.00 |
| proton abstraction mutants |  |  |  |  |
| K131A | 55.4 | 4.7 | 84.0 | 1.24 |
| K133A | 50.6 | −0.2 | 97.4 | −0.05 |
| K235A | 48.5 | −2.2 | 64.5 | −0.59 |
| K131A/K133A | 54.3 | 3.6 | 83.4 | 0.95 |
| K131A/K133A/K235A | 47.9 | −2.9 | 73.0 | −0.77 |
| metal coordination mutants |  |  |  |  |
| D161A | 53.9 | 3.2 | 114.7 | 0.85 |
| E190A | 66.7 | 15.9 | 100.6 | 4.23 |
| D213A | 52.5 | 1.7 | 90.5 | 0.46 |
| D161A/E190A/D213A | 57.4 | 6.7 | 72.2 | 1.77 |
| complete module mutant |  |  |  |  |
| K131A/K133A/D161A/ E190A/D213A/K235A (3KDED) | 64.6 | 13.8 | 87.5 | 3.68 |

[a] In addition to using the method of Schellman (28) for calculating the $\Delta\Delta G_u$ values of these mutants, the method of Gibbs and Helmholtz was also used to find the change in free energy of unfolding using the equation $\Delta G = \Delta H_{wt} - T\Delta S_{wt} + \Delta C_p[T - T_{wt} - T \ln(T/T_{wt})]$. Both methods yielded similar values.

Table 2: Data Collection and Structural Refinement Statistics

| | |
|---|---|
| no. of reflections | 48414 |
| data cutoff | 0 |
| resolution range (Å) | 70−2.3 |
| $R_{work}/R_{free}$ | 0.22/0.29 |
| $I/\sigma(I)$ | 8.4 (1) |
| completeness (%) | 97.46 |
| redundancy | 3.7 |
| $R_{merge}$ (%) | 13 |
| no. of atoms per asymmetric unit | 9608 |
| average $B$-factor, protein atoms (Å$^2$) | 41.1 |
| average $B$-factor, solvent atoms (Å$^2$) | 37.6 |

to the data using a two-state analysis program (27), and each method gave a similar $T_M$ of 50.8 °C (Table 1) and 52.7 °C, respectively (data not shown). When the sample was cooled, 80−90% of the original CD signal (for completely folded enzyme) was recovered, and refolding curves showed a transition temperature that was similar to the melting temperature (data not shown). In addition, the $T_M$ was found to be robust and consistent among different rates of sample heating. The $\Delta H_{VH}$ of the wild-type enzyme was calculated to be 86.1 kcal, which is consistent with other reported values for $(\beta/\alpha)_8$-barrel proteins (36).

*Thermal Denaturation of OSBS Mutants.* OSBS alanine-substituted mutants were reversibly denatured by temperature and analyzed by far-UV CD. The loss of helical content was fit as described for the wild-type enzyme. When the sample was cooled, 80−90% of the original CD signal was recovered. The calculated $T_M$, $\Delta\Delta G_u$, and $\Delta H_{VH}$ of each alanine-substituted mutant are listed in Table 1. Although most substitutions either caused a negligible change in melting temperature or stabilized the protein, the K235A mutant exhibited a lower melting temperature, indicating that this substitution is destabilizing.

*Determination of $\Delta C_p$ for Wild-Type OSBS and the E190A and 3KDED Mutants.* The nonadditive stabilization effects in the 3KDED mutant and the magnitude of the difference in melting temperature between the E190A and 3KDED

mutants and the wild-type enzyme raise the question of whether the thermostability changes we observed are consistent over a wide temperature range. To address this question, the $\Delta C_p$ was determined for wild-type OSBS, the E190A mutant, and the 3KDED mutant by performing reversible thermal denaturations in the presence of varying concentrations of urea (Figure 3). The calculated $\Delta C_p$ of wild-type OSBS is 3.2 kcal mol$^{-1}$ K$^{-1}$, in accord with the predicted $\Delta C_p$ for a protein of this size (37). In comparison, the calculated $\Delta C_p$ of the E190A mutant was 3.4 kcal mol$^{-1}$ K$^{-1}$. The calculated $\Delta C_p$ for the 3KDED mutant was 3.2 kcal mol$^{-1}$ K$^{-1}$.

*X-ray Crystallographic Structure Determination.* The E190A mutant structure refinement statistics are given in Table 2. The model is not complete, with several side chains and two external loops (residues 13−24 and 111−127) showing very poor or no electron density at all, presumably due to disorder. No bound metal was observed in the active site. The mutant site was clearly visible in the map, with density truncated at the C$\beta$ atom and backbone stereochemistry consistent with alanine rather than glutamate in that position. An attempt to fit the apo model in the mutant map resulted in strong negative density around the E190 side chain and distorted torsion angles for this residue (to avoid clashes with neighboring glutamate side chains). Nevertheless, the structure superimposed well with the wild-type apo structure, retaining the overall $(\beta/\alpha)_8$-barrel fold with an overall rmsd of 0.55 Å over 292 α-carbon atom pairs. In this superposition, no significant distortion of the other residues in the catalytic module was observed.

## DISCUSSION

*Stabilized Mutants.* As predicted by theory, the majority of the alanine substitutions in the OSBS catalytic module resulted in proteins with higher melting temperatures. Many of these melting temperature changes were similar in magnitude to those reported in other studies of function−stability trade-offs. Shoichet et al. (3) report increases in melting temperature of up to 5.1 °C ($\Delta\Delta G_u$ of 2.0 kcal/mol) upon substitution of single catalytic residues in lysozyme. Kanzaki et al. (36) report an increased melting temperature of 4 °C upon substitution of a phenylalanine for a catalytic glutamic acid in the core of tryptophan synthase, another $(\beta/\alpha)_8$-barrel protein. Point mutants K131A, D161A, and D213A all show increases in melting temperature and $\Delta\Delta G_u$ within this range (Table 1).

The circular dichroism experiments were performed in the absence of metal added to the buffer. The results suggest that the presence of metal was unlikely as circular dichroism experiments with OSBS in the presence of metal led to irreversible denaturation (data not shown). Although metal cofactors are required for catalysis by members of the enolase superfamily, substantial evidence from calorimetry experiments and structural characterization of other members of the superfamily suggests that these enzymes are stable and show little distortion of their active sites in the absence of metal (38−40). Similarly, as noted below in the comparison between a structure of wild-type OSBS (determined with metal present) and our structure of the E190A mutant, the absence of metal does not have a significant effect on the geometry of the active site or the overall structure.

Notably, the point mutant E190A has a melting temperature that is 15.9 °C higher than that of wild-type OSBS. This stabilization ($\Delta\Delta G_u = 4.23$ kcal/mol) is far greater than that seen in other alanine-substituted OSBS mutants and is also extremely high relative to previously reported single-mutant values in other systems. Other increases in melting temperature comparable in magnitude have required multiple mutations. For example, Pantoliano et al. (*38*) report an increase of 14.3 °C ($\Delta\Delta G_u = 3.80$ kcal/mol) for a six-mutation subtilisin mutant. Additionally, Matsumura et al. describe a lysozyme mutant that required three engineered disulfide bridges to increase the melting temperature by 23.4 °C (*39*).

Inspection of the wild-type OSBS structure suggests that this stabilization may result from the relief of electrostatic repulsion. E190 is located between D161 and D213, the two other negatively charged metal-coordinating residues, and presumably causes electrostatic repulsion with both (Figure 2). While negatively charged residues D161 and D213 are close to the positively charged residues K133 and K235, respectively (Figure 2), E190 is not close to any positively charged residues that could mitigate this effect through stabilizing interactions. In addition, analysis of the wild-type OSBS structure suggests that the side chains of E190 and D213 clash in several rotameric conformations. Given that the mutation to alanine truncates the side chain, these clashes are not predicted to occur in the E190A mutant structure. Thus, it is not surprising that removing the uncompensated negative charge from E190 greatly stabilizes the protein.

Analysis of the E190A crystal structure suggests that the substitution to alanine relieves some strain in the active site, as the carboxylic side chain of D213 has shifted 0.5 Å closer to the space once occupied by E190 in the wild-type structure (Figure 2). However, it is noteworthy that there is otherwise little structural change in the overall architecture of the active site between the wild type and stabilized mutant, suggesting that the structure of the barrel is robust against destabilization.

If stability and function trade-offs in OSBS were directly correlated, one may wonder whether E190 is the most catalytically important residue since its mutation to alanine makes it the most stable of the mutants we analyzed. We also note that E190 is the single most highly conserved residue in the enolase superfamily, highlighting its contribution to the catalytic module (*40*). Although these experiments cannot determine whether E190 is the "most" catalytically important residue for function in OSBS (as all residues are necessary for function), its obligate conservation suggests that it may play a role in the module that is the least accommodating of change across the members of the superfamily. Viewing our results for OSBS within the context of the superfamily suggests a relationship between global enzyme destabilization and functional necessity associated with this catalytic module residue in all members of the superfamily.

Analysis of mutants in which groups of catalytic module residues are removed (representing the two catalytic subsystems described above) shows that the substitution of additional catalytic residues does not increase stability in an additive manner. This is not surprising, as only substituting residues that are not interacting with each other would likely lead to additive effects (*41*). In sum, this observation supports prior reports that the catalytic module residues interact as two systems with nonadditive effects on stability.

To obtain an estimate of the impact of the entire catalytic module on global enzyme stability, all six residues of the module were mutated to alanine in the mutant 3KDED. 3KDED melts at a temperature that is far greater than that of the wild-type enzyme (Table 1). The stability of this catalytically "empty" $(\beta/\alpha)_8$-barrel mutant is similar to that of a computationally designed active site-less $(\beta/\alpha)_8$-barrel protein which was designed to fold stably (but without a function) (64.6 °C for the 3KDED mutant as compared to 65 °C for the designed protein) (*42*). This comparison between the similar catalytically empty $(\beta/\alpha)_8$-barrels and the wild-type OSBS suggests the stability cost of the catalytic module.

Notably, the temperature stabilization of the 3KDED mutant is smaller than that of the E190A mutant ($\Delta T_M$ values of 13.8 and 15.9 °C and $\Delta\Delta G_u$ values of 3.68 and 4.23 kcal/mol relative to wild-type OSBS, respectively). As removing other components of the system besides E190 does not yield an additive gain in stability, this may indicate that the additional components of the system do not incur a greater cost in destabilization then that incurred by the presence of E190 alone. Thus, these results suggest one possible reason why the catalytic module has been so widely used in the evolution of new function; the organization of the module perhaps supports the insertion of the several functionally important residues conserved in the active site without concomitant additive losses in stability. Through such a strategy, variations in the active site can be achieved while retaining a minimum level of stability necessary for folding or to accommodate additional functional mutations that may be required for specific reactions in the superfamily.

*Destabilized Mutants.* Although the majority of the alanine substitution mutations resulted in proteins with higher melting temperatures, some mutations actually destabilize the protein. Most notably, both mutants that contain a lysine to alanine mutation at position 235 (K235A and K131A/K133A/K235A) are less stable than the wild-type enzyme. Interestingly, when paired with a stabilized alanine substitution mutant (K131A/K133A, $\Delta T_M = 3.6$ °, $\Delta\Delta G_u = 0.95$ kcal/mol), the K235A mutation dominates the stability profile, leading to a mutant that is destabilized relative to the wild type ($\Delta\Delta G_u = -0.77$ kcal/mol).

K235 has been deemed to be critical for proton abstraction in OSBS because mutation to alanine, serine, or arginine obviates both exchange of the $\alpha$-proton with solvent deuterium and the subsequent dehydration step (*23*). While mechanistic roles for structural homologues of K235 have been characterized in some superfamily members (*43, 44*), the role of this residue has not been conclusively determined in the catalytic mechanism of OSBS (*23*). Because K235 is a charged residue in the enzyme core (*13*), we would predict that it would be destabilizing and is conserved because of its contribution to function. Thus, it is surprising to find that removal of the residue's charge (through mutation to alanine) is destabilizing.

Inspection of the crystal structure of wild-type OSBS suggests several reasons why the K235A mutant may be destabilized. Although past work by Stites et al. (*45*) has

indicated that the methylene groups in the lysine side chain can pack within a hydrophobic core, this packing is dependent on the lysine being deprotonated. Given that continuum electrostatics methods have predicted that the structurally analogous lysine in related family members has a high upward $pK_a$ shift (*13*), it is unlikely that K235 is deprotonated and able to make significant packing interactions in OSBS. Instead, the destabilization is likely due to the removal of a salt bridge between the positively charged K235 and a conserved aspartate residue at position 213 (D213) (the distance between the side chains of K235 and D213 is approximately 3 Å). Upon removal of the stabilizing salt bridge in the K235A mutant, residue D213 may then shift closer to its metal-coordinating partner glutamate 190 (E190). This shift may cause all three acidic metal coordinating residues to be closer in space, thereby destabilizing the global structure (Figure 2).

In our experimental system, these observations suggest that the conservation of K235 contributes to global stability in the context of the catalytic module, thus rationalizing its requirement for functional activity and suggesting an additional dimension to the relationship between structure and function in this catalytic module; some residues may be catalytically essential because they stabilize other catalytic residues.

*Applications for Protein Design and Engineering.* These results have potentially important implications with regard to protein design and engineering. Since protein stability is predicted to be a limiting factor in the evolution of novel function (*7, 9, 46*), both the E190A and 3KDED mutants could potentially be used as platforms for protein engineering in $(\beta/\alpha)_8$-barrels. The overall stability and higher melting temperature of the 3KDED mutant give a foundation for estimating the upper limit of the underlying stability of a $(\beta/\alpha)_8$-barrel fold after an active site is removed. This limit agrees well with that defined for a $(\beta/\alpha)_8$-barrel designed without an active site (*42*). This suggests that the biophysical measurements derived from comparing the stabilities of the empty 3KDED protein and the functional wild-type OSBS may be useful in predicting the level of destabilization that can be tolerated by an empty (no active site) $(\beta/\alpha)_8$-barrel protein. Additionally, the crystal structure of the E190A mutant verifies that removal of the most destabilizing element does not change the architecture around the active site, indicating that perhaps other catalytic modules could be placed into the robust OSBS framework for engineering new function. In sum, this study suggests that the OSBS scaffold may provide a useful and general system for the design of new active sites within $(\beta/\alpha)_8$-barrel protein scaffolds.

## CONCLUSIONS

Investigation of the single and combinatorial contributions of the enolase superfamily catalytic module residues to structural stability and enzymatic function extends previous observations of the trade-offs between enzyme stability and function. Principally, this allows us to view the problem within the context of a critical set of residues required for catalysis among all members of a large and mechanistically diverse superfamily. Our results show a nonadditive increase in stability when the components of the catalytic module are

altered, which supports prior work describing the function of the module as an interacting system (*17*). Within this system, we have identified the components that make the greatest contributions to destabilization, as well as functionally essential residues that actually stabilize the global structure, suggesting refinement to simple theories for explaining the stability−function trade-off in enzyme active sites. To the extent that our results for the *E. coli* OSBS can be generalized to the entire enolase superfamily, we can propose a new explanation for nature's repeated use of this catalytic module in the evolution of a large number of different enzymatic reactions.

## REFERENCES

1. Beadle, B. M., and Shoichet, B. K. (2002) Structural bases of stability-function tradeoffs in enzymes, *J. Mol. Biol. 321*, 285−296.
2. Benkovic, S. J., and Hammes-Schiffer, S. (2003) A perspective on enzyme catalysis, *Science 301*, 1196−1202.
3. Shoichet, B. K., Baase, W. A., Kuroki, R., and Matthews, B. W. (1995) A relationship between protein stability and protein function, *Proc. Natl. Acad. Sci. U.S.A. 92*, 452−456.
4. Wang, X., Minasov, G., and Shoichet, B. K. (2002) Evolution of an antibiotic resistance enzyme constrained by stability and activity trade-offs, *J. Mol. Biol. 320*, 85−95.
5. Meiering, E. M., Serrano, L., and Fersht, A. R. (1992) Effect of active site residues in barnase on activity and stability, *J. Mol. Biol. 225*, 585−589.
6. Schreiber, G., Buckle, A. M., and Fersht, A. R. (1994) Stability and function: Two constraints in the evolution of barstar and other proteins, *Structure 2*, 945−951.
7. Bershtein, S., Segal, M., Bekerman, R., Tokuriki, N., and Tawfik, D. S. (2006) Robustness-epistasis link shapes the fitness landscape of a randomly drifting protein, *Nature 444*, 929−932.
8. Besenmatter, W., Kast, P., and Hilvert, D. (2004) New enzymes from combinatorial library modules, *Methods Enzymol. 388*, 91−102.
9. Bloom, J. D., Labthavikul, S. T., Otey, C. R., and Arnold, F. H. (2006) Protein stability promotes evolvability, *Proc. Natl. Acad. Sci. U.S.A. 103*, 5869−5874.
10. Dodson, G., and Wlodawer, A. (1998) Catalytic triads and their relatives, *Trends Biochem. Sci. 23*, 347−352.
11. Gerlt, J. A., and Babbitt, P. C. (2001) Divergent evolution of enzymatic function: Mechanistically diverse superfamilies and functionally distinct suprafamilies, *Annu. Rev. Biochem. 70*, 209−246.
12. Elcock, A. H. (2001) Prediction of functionally important residues based solely on the computed energetics of protein structure, *J. Mol. Biol. 312*, 885−896.
13. Livesay, D. R., Jambeck, P., Rojnuckarin, A., and Subramaniam, S. (2003) Conservation of electrostatic properties within enzyme families and superfamilies, *Biochemistry 42*, 3464−3473.
14. Livesay, D. R., and La, D. (2005) The evolutionary origins and catalytic importance of conserved electrostatic networks within TIM-barrel proteins, *Protein Sci. 14*, 1158−1170.
15. Gerlt, J. A., Babbitt, P. C., and Rayment, I. (2005) Divergent evolution in the enolase superfamily: The interplay of mechanism and specificity, *Arch. Biochem. Biophys. 433*, 59−70.
16. Babbitt, P. C., Mrachko, G. T., Hasson, M. S., Huisman, G. W., Kolter, R., Ringe, D., Petsko, G. A., Kenyon, G. L., and Gerlt, J. A. (1995) A functionally diverse enzyme superfamily that abstracts the α protons of carboxylic acids, *Science 267*, 1159−1161.
17. Babbitt, P. C., Hasson, M. S., Wedekind, J. E., Palmer, D. R., Barrett, W. C., Reed, G. H., Rayment, I., Ringe, D., Kenyon, G. L., and Gerlt, J. A. (1996) The enolase superfamily: A general

strategy for enzyme-catalyzed abstraction of the α-protons of carboxylic acids, *Biochemistry 35*, 16489−16501.

18. Esaki, N., and Walsh, C. T. (1986) Biosynthetic alanine racemase of *Salmonella typhimurium*: Purification and characterization of the enzyme encoded by the alr gene, *Biochemistry 25*, 3261−3267.

19. Glavas, S., and Tanner, M. E. (1999) Catalytic acid/base residues of glutamate racemase, *Biochemistry 38*, 4106−4113.

20. Herron, S. R., Benen, J. A., Scavetta, R. D., Visser, J., and Jurnak, F. (2000) Structure and function of pectic enzymes: Virulence factors of plant pathogens, *Proc. Natl. Acad. Sci. U.S.A. 97*, 8762−8769.

21. Scavetta, R. D., Herron, S. R., Hotchkiss, A. T., Kita, N., Keen, N. T., Benen, J. A., Kester, H. C., Visser, J., and Jurnak, F. (1999) Structure of a plant cell wall fragment complexed to pectate lyase C, *Plant Cell 11*, 1081−1092.

22. Sharma, V., Meganathan, R., and Hudspeth, M. E. (1993) Menaquinone (vitamin K2) biosynthesis: Cloning, nucleotide sequence, and expression of the menC gene from *Escherichia coli*, *J. Bacteriol. 175*, 4917−4921.

23. Klenchin, V. A., Taylor Ringia, E. A., Gerlt, J. A., and Rayment, I. (2003) Evolution of enzymatic activity in the enolase superfamily: Structural and mutagenic studies of the mechanism of the reaction catalyzed by o-succinylbenzoate synthase from *Escherichia coli*, *Biochemistry 42*, 14427−14433.

24. Rieger, C. E., and Turnbull, J. L. (1996) Small scale biosynthesis and purification of gram quantities of chorismic acid, *Prep. Biochem. Biotechnol. 26*, 67−76.

25. Palmer, D. R., Garrett, J. B., Sharma, V., Meganathan, R., Babbitt, P. C., and Gerlt, J. A. (1999) Unexpected divergence of enzyme function and sequence: "N-Acylamino acid racemase" is o-succinylbenzoate synthase, *Biochemistry 38*, 4252−4258.

26. Popp, J. L., Berliner, C., and Bentley, R. (1989) Vitamin K (menaquinone) biosynthesis in bacteria: High-performance liquid chromatographic assay of the overall synthesis of o-succinylbenzoic acid and of 2-succinyl-6-hydroxy-2,4-cyclohexadiene-1-carboxylic acid synthase, *Anal. Biochem. 178*, 306−310.

27. Kirchhoff, W. (1993) National Institute of Standards and Technology Technical Note 1401, U.S. Department of Commerce Technology Administration, Washington, DC.

28. Becktel, W. J., and Schellman, J. A. (1987) Protein stability curves, *Biopolymers 26*, 1859−1877.

29. Leslie, A. G. W. (1992) Recent changes to the MOSFLM package for processing film and image plate data, *Joint CCP4 + ESF-EAMCB Newsletter on Protein Crystallography 26*.

30. Collaborative Computational Project Number 4 (1994) The CCP4 Suite: Programs for Protein Crystallography, *Acta Crystallogr. D50*, 760−763.

31. Vagin, A., and Teplyakov, A. (1997) MOLREP: An automated program for molecular replacement, *J. Appl. Crystallogr. 30*, 1022−1025.

32. Murshudov, G. N., Vagin, A. A., and Dodson, E. J. (1997) Refinement of macromolecular structures by the maximum-likelihood method, *Acta Crystallogr. D53*, 240−255.

33. Perrakis, A., Morris, R., and Lamzin, V. S. (1999) Automated protein model building combined with iterative structure refinement, *Nat. Struct. Biol. 6*, 458−463.

34. Emsley, P., and Cowtan, K. (2004) Coot: Model-building tools for molecular graphics, *Acta Crystallogr. D60*, 2126−2132.

35. Winn, M. D., Isupov, M. N., and Murshudov, G. N. (2001) Use of TLS parameters to model anisotropic displacements in macromolecular refinement, *Acta Crystallogr. D57*, 122−133.

36. Kanzaki, H., McPhie, P., and Miles, E. W. (1991) Effect of single amino acid substitutions at positions 49 and 60 on the thermal unfolding of the tryptophan synthase α subunit from *Salmonella typhimurium*, *Arch. Biochem. Biophys. 284*, 174−180.

37. Dill, K. A., Alonso, D. O., and Hutchinson, K. (1989) Thermal stabilities of globular proteins, *Biochemistry 28*, 5439−5449.

38. Pantoliano, M. W., Whitlow, M., Wood, J. F., Dodd, S. W., Hardman, K. D., Rollence, M. L., and Bryan, P. N. (1989) Large increases in general stability for subtilisin BPN′ through incremental changes in the free energy of unfolding, *Biochemistry 28*, 7205−7213.

39. Matsumura, M., Signor, G., and Matthews, B. W. (1989) Substantial increase of protein stability by multiple disulphide bonds, *Nature 342*, 291−293.

40. Pegg, S. C., Brown, S. D., Ojha, S., Seffernick, J., Meng, E. C., Morris, J. H., Chang, P. J., Huang, C. C., Ferrin, T. E., and Babbitt, P. C. (2006) Leveraging enzyme structure-function relationships for functional inference and experimental design: The structure-function linkage database, *Biochemistry 45*, 2545−2555.

41. Zhang, X. J., Baase, W. A., Shoichet, B. K., Wilson, K. P., and Matthews, B. W. (1995) Enhancement of protein stability by the combination of point mutations in T4 lysozyme is additive, *Protein Eng. 8*, 1017−1022.

42. Offredi, F., Dubail, F., Kischel, P., Sarinski, K., Stern, A. S., Van de Weerdt, C., Hoch, J. C., Prosperi, C., Francois, J. M., Mayo, S. L., and Martial, J. A. (2003) De novo backbone and sequence design of an idealized α/β-barrel protein: Evidence of stable tertiary structure, *J. Mol. Biol. 325*, 163−174.

43. Taylor Ringia, E. A., Garrett, J. B., Thoden, J. B., Holden, H. M., Rayment, I., and Gerlt, J. A. (2004) Evolution of enzymatic activity in the enolase superfamily: Functional studies of the promiscuous o-succinylbenzoate synthase from *Amycolatopsis*, *Biochemistry 43*, 224−229.

44. Landro, J. A., Kallarakal, A. T., Ransom, S. C., Gerlt, J. A., Kozarich, J. W., Neidhart, D. J., and Kenyon, G. L. (1991) Mechanism of the reaction catalyzed by mandelate racemase. 3. Asymmetry in reactions catalyzed by the H297N mutant, *Biochemistry 30*, 9274−9281.

45. Stites, W. E., Gittis, A. G., Lattman, E. E., and Shortle, D. (1991) In a staphylococcal nuclease mutant the side-chain of a lysine replacing valine 66 is fully buried in the hydrophobic core, *J. Mol. Biol. 221*, 7−14.

46. Besenmatter, W., Kast, P., and Hilvert, D. (2007) Relative tolerance of mesostable and thermostable protein homologs to extensive mutation, *Proteins 66*, 500−506.

47. Petterson, E. F., Goddard, T. D., Huang, C. C., Couch, G. S., Greenblatt, D. M., Meng, E. C., and Ferrin, T. E. (2004) UCSF Chimera: A Visualization System for Exploratory Research and Analysis, *J. Comput. Chem. 25*, 1605−1612.